Discrete tomographic reconstruction from deliberately motion blurred X-ray projections

Wim van Aarle[1], Jeroen Cant[1,2], Jan De Beenhouwer[1], Jan Sijbers[1]

[1] iMinds - Vision Lab, University of Antwerp, Wilrijk, Belgium

[2] Agfa Healthcare NV, Mortsel, Belgium

Abstract

An X-ray scanning procedure in which the source and detector rotate continuously has many advantages with respect to scanning stability and scanning speed. However, in such an acquisition scheme, the acquired projections are motion blurred, which should be accounted for. Recently, a method was developed to reconstruct images from motion blurred projections [1]. In this work, we extend this method towards discrete tomography in which prior knowledge about the attenuation values of the object to be scanned is exploited. Results show that by doing so, more details of the object can be obtained, especially further away from the centre of rotation.

Keywords: computed tomography, continuous projections, discrete tomography

1 Introduction

Many Computed Tomography (CT) applications benefit from a reduction in total scan time. Not only does this lead to a lower radiation dose, it also allows the reconstruction of dynamic processes. Many current CT setups follow a step-and-shoot acquisition mode in which the X-ray source and detector (or the object in fixed source/detector systems) are kept still during the exposure of the projection measurement. However, when the rotation speed is pushed to the limits of the system, reconstruction quality will decrease. In systems with a fixed source/detector pair and a rotating object, the short bursts of acceleration and deceleration of the rotation stage are likely to induce small object movement, leading to alignment artefacts in the reconstruction. On systems with a fixed object and a rotating source/detector pair, precisely controlling the X-ray source and detector in between two exposures is challenging and often results in an unstable focal spot, again leading to blurry reconstructed images. Moreover, on very fast scans, detector lag or afterglow can result in projection images that partly contain the signal of the previous exposures [2]. Therefore, fast but accurate scans can then only be taken if the number of projection images is significantly reduced, in turn leading to an insufficient data reconstruction problem, which is known to be hard to solve unless prior knowledge about the object is available [3].

An alternative acquisition strategy is to keep the X-ray source and detector (or the object, depending on the type of system) in a constant motion during measurements. This continuous acquisition mode allows very fast and stable acquisition, but suffers from motion blurred projection data as each measurement on a detector is made up of information on a range of project angles. In effect, this deliberately induces artefacts similar to those of detector afterglow. Without any correction or advanced system modelling, the use of a continuous acquisition scheme can therefore only be considered if many projections are taken (i.e. if the detector data are read out at a high frequency), as the data then approximates that of a conventional step-and-shoot acquisition. The paradox of continuous acquisition is thus that it can lead to fast acquisitions, but offer accurate results only if it is performed slowly. Recently however, an approach has been proposed in which the angular blurring effect of the continuous acquisition model is integrated into the reconstruction framework [1]. It was shown that even with a low number of projection images (i.e. with fast acquisition) highly accurate reconstruction quality can be obtained around the centre of rotation. Outside of this region, however, this approach offers improved radial resolution but also a decreased tangential resolution.

In this work, we explore the benefit of exploiting prior knowledge about the scanned object to further increase the area in which accurate reconstructions can be acquired. The Discrete Algebraic Reconstruction Technique (DART) is a technique that has proven to be very powerful when accurate information about the objects materials is available [3].

2 Method

2.1 Step-and-shoot acquisition mode

Consider a single step-and-shoot projection measurement of an object represented by the attenuation values $\mu(x, y)$:

$$I_i^s(t) = I_0 exp\left(-\int_{L_{t,\theta}} \mu(x,y)ds\right),$$

where I_0 denotes is the incident beam intensity and $L_{t,\theta} = \{(x,y)|xcos\theta + sin\theta = t\}$ denotes the line corresponding to the i'th measurement of the scanned data.

Let $\boldsymbol{v} \in \mathbb{R}^n$ denote the unknown rasterized representation of the object function, and let $\boldsymbol{p} \in \mathbb{R}^{ld}$ denote the measured projection data with l the number of projection angles and d the number of detector pixels in each projection. Define the function $\omega_{\theta,t}: \mathbb{R}^n \to \mathbb{R}$ as the projection function of an object under a certain angle θ at a certain detector position t. Using Beer-Lamberts law, the projection formula can then be linearized to

$$p_i = -ln\left(\frac{I_i^s(r)}{I_0}\right) = \int_{L_{t,\theta_n}} \mu(x,y)ds = \omega_{\theta,t}(\boldsymbol{v})$$

Let $\boldsymbol{W^s} \in \mathbb{R}^{ld\times n}$ represent the projection matrix of the scanning geometry, i.e. let each value w_{ij} represent the contribution of volume pixel j to detector pixel i. The projection function can then be expressed as a linear combination of all pixels in the volume:

$$\omega_{\theta,t}(\boldsymbol{v}) = \sum_{j=1}^{n} w_{ij}^s v_j$$

This leads to the linear system of equations

$$\boldsymbol{W^s v} = \boldsymbol{p},$$

that represents the reconstruction problem. It can be solved by many different iterative solvers, such as SART, SIRT [4], or the Krylov subspace method CGLS [5].

2.2 Continuous acquisition mode

For continuous acquisition, each projection exposure k, that includes measurement i, is equivalent to all integrated exposures in the range $[\theta_k, \theta_{k+1}]$:

$$I_i^c(t) = \frac{I_0}{\Omega}\int_{\theta_k}^{\theta_{k+1}} exp\left(-\int_{L_{t,\alpha}} \mu(x,y)ds\right)d\alpha,$$

with Ω a normalization parameter. The continuous motion can be approximated by sampling the projection space in the range $[\theta_k, \theta_{k+1}]$ using S samples, equiangularly spaced with an interval Δ. Larger values of S, and lower values of Δ, lead to more accurate approximations, but result in a larger computation burden to compute the reconstruction. Using this discretization by sampling, combined with Beer-Lambert's law, the continuous projection model can be written as

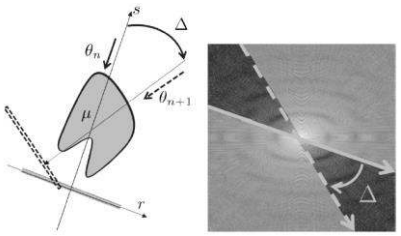

1. (a) (b)

Figure 1: In a continuous projection, the detector integrates photons between θ_k and θ_{k+1}(a) and gathers data about a wedge in the Fourier space (b).

$$p_i = -ln\left(\frac{1}{S}\sum_{s=1}^{S} \exp\left[-\omega_{\theta_k+s\Delta,t}(\boldsymbol{v})\right]\right).$$

Clearly, there is no linear correspondence between the projection data p_i and the volume data v_j. This means that this projection model can not be efficiently solved by conventional reconstruction techniques. The function can be approximated, however, by making an additional assumption on the scanned object, namely that small changes in the projection direction lead only to small changes in the projection measurements [1].

Define $p_{i,s}$ as the virtual step-and-shoot projection at sampling step s, i.e., $p_{i,s} = \omega_{\theta_k+s\Delta,t}(\boldsymbol{v})$. Define $p_{i,avg}$ as the average projection value inside the angular range, i.e., $p_{i,avg} = \frac{1}{S}\sum_{s=1}^{S} p_{i,s}$. The projection measurement is then

$$p_i = -ln\left(\frac{1}{S}\sum_{s=1}^{S} \exp\left[-p_{i,s}\right]\right) = -ln\left(\frac{1}{S}\sum_{s=1}^{S} \exp\left[p_{i,avg} - p_{i,s} - p_{i,avg}\right]\right) = p_{i,avg} - ln\left(\frac{1}{S}\sum_{s=1}^{S} \exp\left[p_{i,avg} - p_{i,s}\right]\right).$$

With $p_{i,avg}$ assumed to be very close to $p_{i,s}$ the fact that for small , $\exp(x) \approx 1 + x$, can be exploited to approximate p_i:

$$p_i \approx p_{i,avg} - ln\left(\frac{1}{S}\sum_{s=1}^{S} 1 + \mathrm{p}_{i,avg} - p_{i,s}\right) = p_{i,avg}$$

Define $\overline{\boldsymbol{W}}^{\boldsymbol{c}} \in \mathbb{R}^{lSd \times n}$ as the projection matrix that simulates forward projections for all d exposures and at all S sampling points. The values $\overline{w}^{c}_{iS+s,j}$ represent the contribution of voxel v_j to measurement p_i at sampling point s inside one continuous projection exposure.

$$p_{i,avg} = \sum_{j=1}^{n} \sum_{s=1}^{S} \overline{w}^{c}_{iS+s,j} v_j$$

Finally, define $\boldsymbol{W}^{\boldsymbol{c}} \in \mathbb{R}^{ld \times n}$ as the projection matrix that simulates d continuous exposure projections. In essence, each row of $\boldsymbol{W}^{\boldsymbol{c}}$ can be regarded as the summation of the S corresponding rows in $\overline{\boldsymbol{W}}^{\boldsymbol{c}}$: $w^{c}_{ij} = \sum_{s=1}^{S} \overline{w}^{c}_{iS+s,j}$ The measured projection in then

$$p_i \approx \sum_{j=1}^{n} w^{c}_{ij} v_j,$$

leading to the linear reconstruction problem

$$\boldsymbol{W}^{\boldsymbol{c}} \boldsymbol{v} \approx \boldsymbol{p},$$

which can be easily solved using conventional reconstruction solvers.

2.3 Discrete Tomography

Conventional algebraic reconstruction solvers search for the reconstructed volume by minimizing some norm. For example, the SIRT method minimizes the weighted projection difference, $\|\boldsymbol{W}^{\boldsymbol{c}} \boldsymbol{v} - \boldsymbol{p}\|^2_{\boldsymbol{R}}$, with $\boldsymbol{R}$ the inverse row sums of $\boldsymbol{W}^{\boldsymbol{c}}$. If sufficient data is available, that is, if the projection matrix is long and thin ($ld > n$), the minimum of this optimization function closely corresponds to the actual object function. For scans with insufficient data, however, it occurs that the reconstruction equation, $\boldsymbol{W}\boldsymbol{v} = \boldsymbol{p}$, holds too many unknowns for the amount of measurements ($ld \ll n$). This insufficient data then typically prevents the solver from converging to an accurate reconstruction. This situation occurs if the projection data is truncated, if projections data is not acquired from all directions, and if only a few projection images are acquired. When dealing with very fast scans, both the step-and-shoot and continuous exposure models fall into this last category. In step-and-shoot data, high quality projection information is known from only a few directions. In continuous exposure data, however, low quality projection information from all angles is recorded, but is hidden inside only a few detector readouts.

A common solution to counter insufficient data problems is to exploit available prior knowledge about the scanned object. The Discrete Algebraic Reconstruction Technique (DART) uses information about the object densities, and interleaves segmentation phases with reconstruction update phases limited to the pixels near the edge of the segmentation (see Fig. 2) [3]. That way, the reconstruction problem in each DART iteration is smaller in size and thus easier to solve, eventually leading to very accurately segmented reconstructions.

1. Compute an initial SIRT reconstruction, $\boldsymbol{v}^{(\boldsymbol{0})}$. Set $k = 0$.
2. Create a segmentation $\boldsymbol{s}^{(\boldsymbol{k})}$of $\boldsymbol{v}^{(\boldsymbol{k})}$ by applying (e.g., a global thresholding) segmentation function $\mathcal{L}_{\tau,\rho}$, where ρ represents the grey level values corresponding to the attenuation values of each distinct material present in the scanned object, and τ represents the threshold values in between them. If k is zero or a multiple of 5, automatically update τ and ρ by minimizing the projection difference between the segmentation and the measured data [6]:
$$\hat{\tau}, \hat{\rho} = argmin_{\tau,\rho} \left\| \boldsymbol{W}^{\boldsymbol{c}} \mathcal{L}_{\tau,\rho}(\boldsymbol{v}^{(\boldsymbol{k})}) - \boldsymbol{p} \right\|$$
3. Compute $\boldsymbol{f}^{(\boldsymbol{k})}$ identical to $\boldsymbol{s}^{(\boldsymbol{k})}$, but set all pixels that are near the boundary of the segmented object to 0. The grey levels of the nen-zero pixels are considered to be correct in this iteration.
4. Compute the residual $\boldsymbol{r}^{(\boldsymbol{k})} = \boldsymbol{p} - \boldsymbol{W}^{\boldsymbol{c}} \boldsymbol{f}^{(\boldsymbol{k})}$. Assuming that all inner pixels were segmented correctly, the residual data is the projection data that matches all pixels near the edges of the current segmentation.
5. Compute a SIRT reconstruction of $\boldsymbol{r}^{(\boldsymbol{k})}$, limited to the pixels near the boundary of the current segmented objects. This new reconstruction uses the same number of equations to solve a substantially lower number of unknowns, and is thus more likely to result in an accurate reconstruction. Set $\boldsymbol{v}^{(\boldsymbol{k+1})}$ to $\boldsymbol{s}^{(\boldsymbol{k})}$, and update it with the new SIRT reconstruction.
6. Increase k by 1 and return to step 2 until a convergence criterion is met.

Figure 2: Steps of the iterative Discrete Algebraic Reconstruction Technique (DART) as used in Section 3 of this work [3,6].

3 Experiment

To demonstrate the effect of prior knowledge exploitation on continuous projections, consider a 512x512 binary phantom image (Fig.3a) containing 160 circles with a 10 pixel diameter. Parallel beam projection data were simulated with a range of projection exposure counts, both with a step-and-shoot and a continuous acquisition model. The sampling factor S was set to 50. To simulate low radiation and low exposure time scans, Poisson noise was applied with an incident photon count of only $I_0 = 2500$. The open source ASTRA Toolbox [7] was used to compute 300-iteration SIRT and 100-iteration DART reconstructions. Fig.3 shows reconstructions for the case of 20 projection exposures. For validation, the root-mean-square-errors were computed of all reconstructions inside three different areas: close to the centre of rotation (inner), extended (middle) and the full volume (outer) (see Fig3.a). The SIRT reconstructions were first segmented using Otsu's thresholding method. Fig.4 shows the results of this experiment.

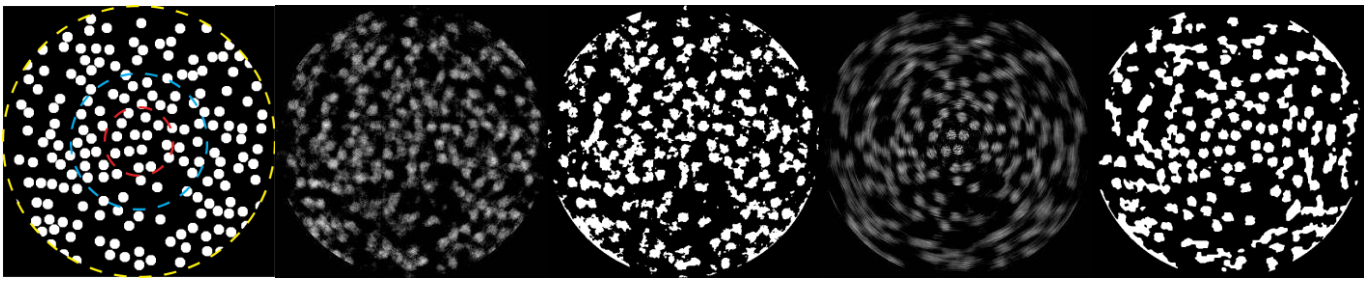

(a) phantom (b) SIRT, step-and-shoot (c) DART, step-and shoot (d) SIRT, continuous (e) DART, continuous

Figure 3: (a) Binary phantom image. Note that three circular areas are marked (inner, middle, outer). (b-e) Reconstructions with 20 projection exposures with all the discussed acquisition and reconstruction models.

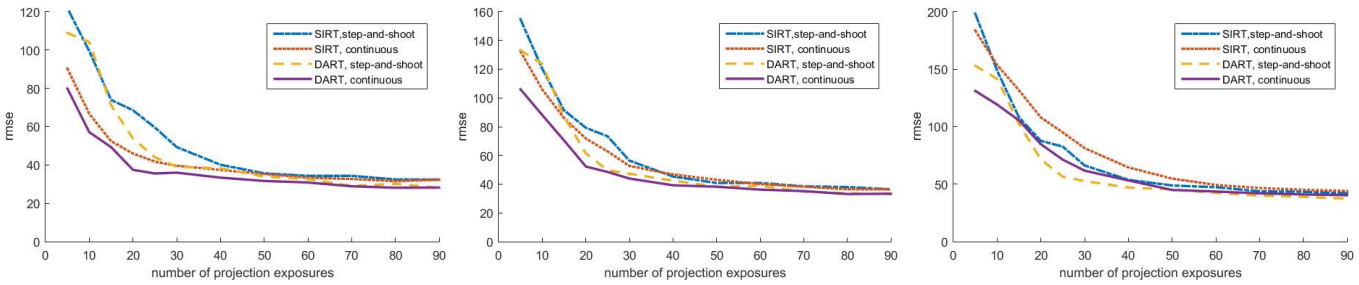

(a) inner circle (b) middle circle (c) outer circle

Figure 4: Root-mean-square-error in three different areas all the discussed acquisition and reconstruction models as a function of angle count.

Considering Fig.3, one can clearly see that near the centre, the reconstruction quality of the continuous acquisition is of a much higher quality than that of the step-and-shoot approach. However, near the edge of the volume, the opposite is true. Due to the high noise component in the projection data, the application of DART provides little benefit to the quality of the step-and-shoot reconstruction. On the other hand, for the continuous reconstructions, DART does prove to be beneficial as more circles, further away from the centre, can be distinguished. The same observations can be seen in Fig.4. For fast, low exposure count, scans continuous acquisition combined with DART clearly provides the best results in the centre of the image. The advantage of DART over SIRT is the largest in the middle circle (Fig.4b), indicating that more circles are indeed reconstructed accurately. As more projection exposures are available, the difference between step-and-shoot and continuous projections decreases and the advantage of continuous projections diminishes. Overall, the results suggest that continuous projections combined with discrete tomography reconstruction can be very beneficial for fast scanning protocols (with a limited number of exposures).

4 Discussion and conclusion

Continuous projection data reveals more accurate reconstructions near the centre of rotation compared to conventional step-and-shoot data because it inherently contains more information (i.e., projections from all directions). This information, however, is collapsed onto each other and to obtain it the acquisition mode has to be taken into account when modelling the forward- and backprojection operators. The implementation presented in this work provides an efficient method to do so, but makes the additional assumption that small changes in the projection direction result in only small changes in the projection

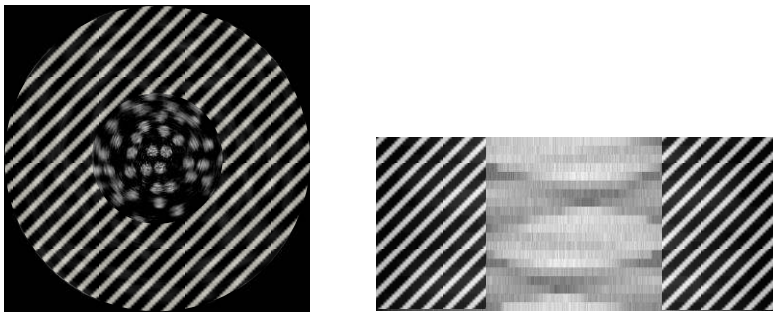

(a) reconstruction (b) sinogram

Figure 5: (a) The outer pixels can not be reconstructed accurately with the proposed approach, as they break an assumption required to be able to use conventional linear solvers to compute the reconstructions. (b) These outer pixels correspond to the most left- and rightward region on the detector array.

data. Whether this assumption is valid depends on the scanned object. Consider a perfect sphere, centred at the centre of rotation. In this case, the assumption fully holds, and the circle can be perfectly reconstructed from only a few continuous projection exposures. On the contrary, consider a single straight line. Here, the projection parallel to the line will have an entirely different shape than the projection just a few degrees away, and accurate reconstruction is not possible [1]. For other objects, the assumption in general holds more for objects that are near the centre of rotation than for those that are further away from it. This explains why the reconstructions from the continuous exposure projections have a location dependent accuracy. Observing that these reconstructions are only accurate in the centre anyway, one can wonder why projection information on these outer regions should be measured in the first place. Indeed, as can be recognized in Fig. 5, the outer parts of the reconstruction correspond only to the most leftward and most rightward region of the detector array. To reduce the radiation dose to the sample, it can thus beneficial to physically reduce the width of the X-ray beam, i.e., to artificially truncate the projection data. To demonstrate, consider Fig.6, in which truncated projection data of the phantom image shown in Fig.3a is reconstructed and compared to a non-truncated projection. Clearly, the reconstruction is very similar inside the region-of-interest (ROI). Outside this ROI, however, the amount of information is now so low that even the exploitation of prior knowledge can not improve the reconstruction quality anymore.

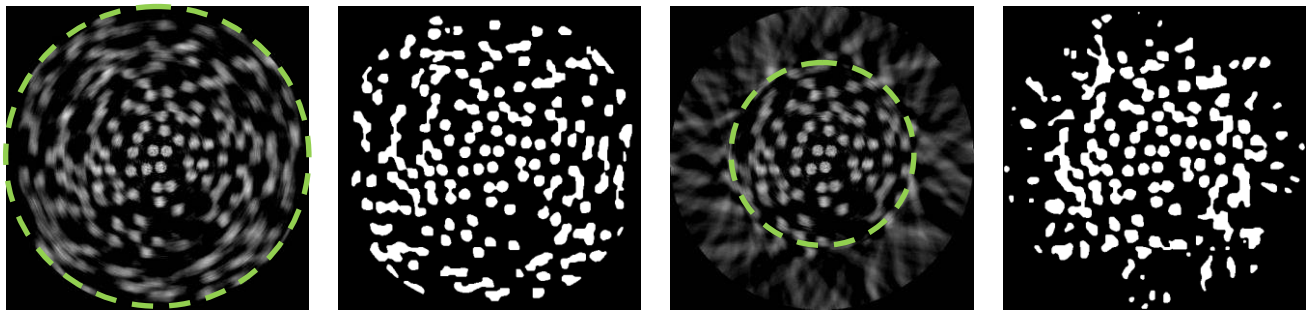

(a) SIRT, no truncation (b) DART, no truncation (c) SIRT, truncated (d) DART, truncated

Figure 6: Reconstructions of Fig.3a from 20 continuous projection exposures. The dashed circle in (a) and (c) denotes the region of interest.

Acknowledgements

The authors wish to acknowledge financial support from the iMinds ICON MetroCT project, and the IWT SBO TomFood project. Networking support was provided by the EXTREMA COST Action MP1207.

References

[1] J. Cant, W. J. Palenstijn, G. Behiels, and J. Sijbers, "Modeling blurring effects due to continuous gantry rotation: application to region of interest tomography", Medical Physics, vol. 42, pp. 2709-2717, 2015.

[2] J. Hsieh, O. E. Gurmen, and F. King, “Investigation of a Solid-State Detector for Advanced Computed Tomography”, IEEE Transactions on Medical Imaging, vol.19, pp. 930-940, 2000.

[3] K. J. Batenburg, and J. Sijbers, "DART: A Practical Reconstruction Algorithm for Discrete Tomography", IEEE Transactions on Image Processing, vol.20, pp. 2542-2553, 2011.

[4] J. Gregor, and T. Benson, “Computational analysis and improvement of SIRT”, IEE Transactions on Medical Imaging, vol.27, pp.918-924, 2008.

[5] P. Gilbert, “Iterative methods for the three-dimensional reconstruction of an object from proejctions.”, Journal of theoretical Biology, vol.36, pp.105-117, 1972.

[6] W. van Aarle, K. J. Batenburg, and J. Sijbers, “Automatic parameter estimation for the Discrete Algebraic Reconstruction Technique”, IEEE Transactions on Image Processing, vol.21, pp. 4608-4621, 2012.

[7] W. van Aarle, W. J. Palenstijn, J. De Beenhouwer, T. Altantzis, S. Bals, K. J. Batenburg, and J. Sijbers, "The ASTRA Toolbox: a platform for advanced algorithm development in electron tomography", Ultramicroscopy, vol. 157, pp. 35-47, 2015.